
Stable and expressive recurrent vision models

Drew Linsley*, Alekh K Ashok*, Lakshmi N Govindarajan*, Rex Liu, Thomas Serre

Carney Institute for Brain Science
 Department of Cognitive Linguistic & Psychological Sciences
 Brown University
 Providence, RI 02912
 {drew_linsley, alekh_ashok, lakshmi_govindarajan,
 rex_liu, thomas_serre}@brown.edu

Abstract

Primate vision depends on recurrent processing for reliable perception [1]. At the same time, there is a growing body of literature demonstrating that recurrent connections improve the learning efficiency and generalization of vision models on classic computer vision challenges. Why then, are current large-scale challenges dominated by feedforward networks? We posit that the effectiveness of recurrent vision models is bottlenecked by the widespread algorithm used for training them, “back-propagation through time” (BPTT), which has $\mathcal{O}(N)$ memory-complexity for training an N step model. Thus, recurrent vision model design is bounded by memory constraints, forcing a choice between rivaling the enormous capacity of leading feedforward models *or* trying to compensate for this deficit through granular and complex dynamics. Here, we develop a new learning algorithm, “contractor recurrent back-propagation” (C-RBP), which alleviates these issues by achieving constant $\mathcal{O}(1)$ memory-complexity with steps of recurrent processing. We demonstrate that recurrent vision models trained with C-RBP can detect long-range spatial dependencies in a synthetic contour tracing task that BPTT-trained models cannot. We further demonstrate that recurrent vision models trained with C-RBP to solve the large-scale *Panoptic Segmentation* MS-COCO challenge outperform the leading feedforward approach. C-RBP is a general-purpose learning algorithm for any application that can benefit from expansive recurrent dynamics. Code and data are available at <https://github.com/c-rbp>.

1 Introduction

Ullman (1984) famously theorized that humans reason about the visual world by composing sequences of elemental computations into “visual routines” [2]. It has been found that many of these visual routines, from perceptual grouping [3] to object categorization [4], depend on local and long-range recurrent circuits of the visual cortex [1, 5, 6]. At the same time, convolutional neural networks (CNNs) with recurrent connections – recurrent CNNs – seem to learn visual routines that standard feedforward CNNs do not [7–14]. For example, consider the *Pathfinder* challenge in Fig. 1, which asks observers to trace the contour extending from the white dot. Although *Pathfinder* is visually simple, clutter and variations in path shape make it difficult for feedforward CNNs to solve, even very deep residual networks [7, 8]. By contrast, a one-layer recurrent CNN can learn to solve *Pathfinder* by incrementally grouping paths from one end to the other, reminiscent of Gestalt-like visual routines used by human observers [7, 8, 15]. Others have found that the visual routines learned by recurrent CNNs on small computer vision datasets lead to better sample efficiency and out-of-distribution generalization than feedforward CNNs [6, 16, 17]. There is also evidence that primate visual decisions and neural

*These authors contributed equally to this work.

responses elicited by natural images are best explained by recurrent CNNs [17–23]. Nevertheless, the great promise of recurrent CNNs has yet to translate into improvements on large-scale computer vision challenges like MS-COCO [24], which are dominated by feedforward CNNs.

A well known limitation of recurrent CNNs is a memory bottleneck imposed by the standard learning algorithm, “back-propagation through time” (BPTT; [25]). The memory requirement of BPTT-trained models scales linearly with steps of processing, since optimization involves propagating error through the full latent trajectory. This makes it difficult to develop recurrent CNNs that can rival the massive capacity of leading feedforward CNNs, which is critical for high performance [26], while also simulating enough steps of processing to learn human-like visual routines that could yield further improvements.

Contributions. We develop a solution to the memory bottleneck introduced by BPTT. Our work is inspired by recent successes in sequence modeling, where memory-efficient approximations to BPTT have performed well [27, 28]. Of particular interest is recurrent back-propagation (RBP), which exploits the stability of convergent dynamical systems to achieve constant memory complexity w.r.t. steps of processing [27, 29, 30]. This approach depends on models with stable dynamics that converge to a task-optimized steady state. However, we find that leading recurrent CNNs violate this assumption and “forget” task information as they approach a steady state. While this pathology can be mitigated with hyperparameters that guarantee stability, these choices hurt model performance, or “expressivity”. Thus, we make the observation that recurrent CNNs face a fundamental trade-off between stable dynamics and model expressivity that must be addressed before they can adopt efficient learning algorithms and compete on large-scale computer vision challenges.

- We derive a constraint for training recurrent CNNs that are both stable *and* expressive. We refer to this as the *Lipschitz-Constant Penalty* (LCP).
- We combine LCP with RBP to introduce “contractor-RBP” (C-RBP), a learning algorithm for recurrent CNNs with constant memory complexity w.r.t. steps of processing.
- Recurrent CNNs trained with C-RBP learn difficult versions of *Pathfinder* that BPTT-trained models cannot due to memory constraints, generalize better to out-of-distribution exemplars, and need a fraction of the parameters of BPTT-trained models to reach high performance.
- C-RBP alleviates the memory bottleneck faced by recurrent CNNs on large-scale computer vision. Our C-RBP trained recurrent model outperforms the leading feedforward approach to the MS-COCO Panoptic Segmentation challenge despite using nearly 800K fewer parameters, and without exceeding the memory capacity of a standard NVIDIA Titan X GPU.

2 Background

We begin with a general formulation of the recurrent update step at $t \in \{1..N\}$ in an arbitrary layer of a recurrent CNN, which processes images with height H and width W .

$$h_{t+1} = F(x, h_t, w_F). \quad (1)$$

This describes the evolution of the hidden state $h \in \mathbb{R}^{H \times W \times C}$ through the update function F (a recurrent layer) with convolutional kernels $w_F \in \mathbb{R}^{S \times S \times C \times C}$, where C is the number of feature channels and S is the kernel size. Dynamics are also influenced by a constant drive $x \in \mathbb{R}^{H \times W \times C}$, which in typical settings is taken from a preceding convolutional layer. The final hidden state activity is either passed to the next layer in the model hierarchy, or fed into an output function to make a task prediction. The standard learning algorithm for optimizing parameters w_F w.r.t. a loss is BPTT, an extension of back-propagation to recurrent networks. BPTT is implemented by replicating the dynamical system in Eq. 1 and accumulating its gradients over N steps (SI Eq. 7). BPTT computes gradients by storing each h_t in memory during the forward pass, which leads to a memory footprint that increases linearly with steps.

Steady state dependent learning rules There are alternatives to BPTT that derive better memory efficiency from strong constraints on model dynamics. One successful example is recurrent back-propagation (RBP), which optimizes parameters to achieve steady-state dynamics that are invariant to slight perturbations of input representations; a normative goal that echoes the classic Hopfield network [31]. When used with models that pass its test of stability, which we detail below, RBP memory complexity is *constant* and does not scale with steps of processing (the precision of dynamics). RBP is especially effective when a system’s steady states can be characterized by determining its Lyapunov function [27]. However, such analyses are generally difficult for non-convex optimizations, and not tractable for the complex loss landscapes of CNNs, especially those

developed for large-scale computer vision challenges, like MS-COCO or ImageNet. RBP assumes that dynamics of the transition function $F(\cdot)$ eventually reach an equilibrium h^* as $t \rightarrow \infty$ (Eq. 2).

$$h^* = F(x, h^*, w_F) \quad (2) \quad \Psi(w_F, h) = h - F(x, h, w_F) \quad (3)$$

In other words, h^* is unchanged by additional processing. We can construct a function $\Psi(\cdot)$ such that the equilibrium h^* becomes its root (Eq. 3); i.e. $\Psi(w_F, h^*) = 0$. RBP leverages the observation that when differentiating Eq. 3, the gradient of steady state activity h^* w.r.t. the parameters of a stable dynamical system w_F can be directly computed with the Implicit Function Theorem [29, 30, 32, 33].

$$\frac{\partial h^*}{\partial w_F} = (I - J_{F, h^*})^{-1} \frac{\partial F(x, h^*, w_F)}{\partial w_F} \quad (4)$$

Here, J_{F, h^*} is the Jacobian matrix $\partial F(x, h^*, w_F) / \partial h^*$ (SI §3). In practice, the matrix $(I - J_{F, h^*})^{-1}$ is numerically approximated [27, 29]. RBP is designed for RNNs that pass its *constraint-qualifications* test for stability, where (i) $\Psi(\cdot)$ is continuously differentiable with respect to w_F and (ii) $(I - J_{F, h^*})$ must be invertible. When these conditions are satisfied, as is often the case with neural networks for sequence modeling, RBP is efficient to compute and rivals BPTT performance [27].

2.1 Do recurrent CNNs pass the constraint-qualifications test of RBP?

We turn to the *Pathfinder* challenge [7, 8] to test whether RBP works for recurrent CNN architectures devised for computer vision. *Pathfinder* is an ideal test bed for recurrent vision models because they can more efficiently solve it than feedforward models. To summarize: (i) *Pathfinder* tests the ability of models to detect long-range spatial dependencies between features – identifying the target contour and tracing it from one end to the other. Since capturing such relationships means that models must have

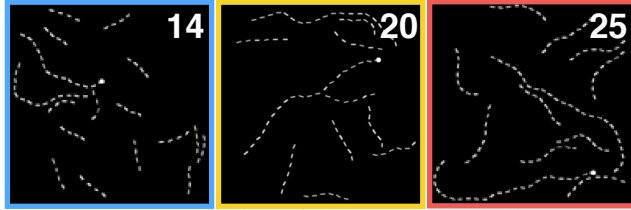


Figure 1: In our variation of the *Pathfinder* challenge [7, 8], we ask observers to segment the contour connected to the white dot. Recurrent CNNs can easily solve it by learning to incrementally “trace” the target from end to end. Target contours are made up of 14-, 20-, or 25-dashes.

units with receptive fields that cover the entire target contour, *Pathfinder* strains the routines that models use to extend their receptive field size. Feedforward architectures (like ResNets) need a sufficient amount of depth to solve difficult versions of this challenge, but this leads to an explosion of parameters which cause learning problems [7, 8]. In contrast, recurrent CNNs can broaden receptive fields over steps of processing without additional processing layers (SI §3), but doing requires maintaining task information across dynamics. (ii) *Pathfinder* is parameterized for fine-grained control over task difficulty. By lengthening or shortening target contours and clutter, we can generate more or less difficult datasets (Fig. 1). (iii) *Pathfinder* controls low-level biases that contaminate natural image datasets [34]. In summary, recurrent CNNs that can solve *Pathfinder* need to learn a robust visual routine for detecting and maintaining long-range spatial dependencies in images. BPTT-trained recurrent CNNs can do this [7, 8]. Here we test whether RBP-trained models can do the same.

Methods We trained the leading recurrent CNN approach for *Pathfinder*, the horizontal gated recurrent unit (hGRU; a complete model description is in SI §3.1), to solve a version where the target contour is 14-dashes long (Fig. 1, left panel). We modified *Pathfinder* from its origins as a classification task [12] to a segmentation task, which makes it easier to interpret model dynamics (e.g., Fig 2), and translate our findings to the large-scale MS-COCO challenge that we investigate in §3.2. The hGRU architecture consisted of (i) an input layer with 24 Gabor-initialized convolutional filters and one difference-of-Gaussians filter, followed by (ii) an hGRU with 15×15 horizontal kernels and 25 output channels, and finally (iii) a 1×1 convolutional “readout” that transformed the final hGRU hidden-state to a per-pixel prediction via batch normalization [35] and a 1×1 convolutional kernel. We began by testing four versions of the hGRU: one trained with BPTT for 6 steps, which was the most that could fit into the 12GB memory of the NVIDIA Titan X GPUs used for this experiment; and versions trained with RBP for 6, 20, and 30 steps. We also trained a fifth control model, a feedforward version of the 6 step BPTT-trained hGRU, where parameters were not shared across time (“feedforward CNN control”). The models were trained with Adam [36] and a learning rate of $3e-4$ to minimize average per-pixel cross entropy on batches of 128 images evenly divided across 4 GPUs.

Training lasted 20 epochs on a dataset of 200,000 images. Performance was measured after every epoch as the mean intersection over union (*IoU*) on a held-out test set of 10,000 images. We report the maximum *IoU* of each model on this test set.

Results The three hGRUs trained with RBP performed poorly on Pathfinder-14 (6 step: 0.50 *IoU*; 20 step: 0.71 *IoU*; 30 step: 0.70 *IoU*), far worse than a BPTT-trained hGRU (0.98 *IoU*). The RBP-hGRUs were also outperformed by the feedforward CNN control (0.78 *IoU*, although this control used 3 times more parameters than the hGRUs).

Why does an hGRU trained with RBP fail to learn *Pathfinder*? To address this question, we return to the constraint-qualifications test of RBP. The hGRU, like all models successfully optimized with gradient descent, satisfies condition (i) of the RBP constraint-qualifications test: it is composed of a series of differentiable functions. This means that the problem likely arises from condition (ii), which requires the matrix $I - J_{F,h^*}$ to be invertible. Indeed, if $I - J_{F,h^*}$ is singular and not invertible, training dynamics will devolve into an unstable regime as we observed for RBP-hGRU training (Fig. S6). One way of guaranteeing an invertible $I - J_{F,h^*}$ is by forcing F to be a contractive map [33]. When this constraint is in place, we can invoke Banach fixed point theorem to ensure convergence to a unique fixed point starting from any initial hidden state h_0 . To elaborate, F implements a contraction map and will converge onto a unique fixed point if the following holds: $\forall h_i, h_j, x$, where $i, j \in \mathbb{R}_+$, $\exists \lambda \in [0, 1)$ such that

$$\|F(h_i; x, w_F) - F(h_j; x, w_F)\|_2 \leq \lambda \|h_i - h_j\|_2 \quad (5)$$

A straightforward way of forcing a contractive map is by building models with hyperparameters that are globally contractive (i.e., across the entire latent trajectory of dynamics), like squashing non-linearities (*sigmoid* and *tanh* [37, 38]). However, these same hyperparameters are suboptimal for computer vision, where unbounded non-linearities (like *ReLU*) are used because of their control over vanishing gradients in deep hierarchical networks and improved function expressivity [39, 40].

In principle, recurrent CNNs like convolutional LSTMs, that use *tanh* non-linearities, should perform better with RBP than an hGRU, which uses soft unbounded rectifications (*softplus*). Indeed, we found that a 20-step convolutional LSTM (“convLSTM”; architecture detailed in SI §3.2) trained with RBP on Pathfinder-14 performs slightly better (0.73 *IoU*) than the RBP-trained hGRU (0.71 *IoU*). At the same time, the RBP-trained convLSTM performs much worse than a 6-step BPTT-trained convLSTM (0.81 *IoU*) and a BPTT-trained hGRU (0.98 *IoU*). In other words, the convLSTM is more stable but less expressive than the hGRU. Furthermore, an hGRU with squashing non-linearities could not be trained reliably with RBP due to vanishing gradients. These findings raise the possibility that recurrent CNNs face a trade-off between “expressivity” needed for competing on large-scale computer vision challenges, and “stability” that is essential for using learning algorithms like RBP which rely on equilibrium dynamics.

Expressivity vs. stability To better understand the trade-off faced by recurrent CNNs, we examined the stability of an expressive recurrent CNN: the BPTT-trained hGRU, which outperformed all other architectures on Pathfinder-14. We performed a state space analysis to visualize its dynamics on all images in the Pathfinder-14 test set (method in SI §3.3). The state space revealed a large divergence between hGRU hidden state activity at the task-optimized $t = 6 = N$ step vs. activity near steady state at $t = 40 = T$ (Fig. 2a). There was nearly as large of a difference between hidden states at $t = N$ and $t = T$ as there was between hidden states at $t = N$ and $t = 1$. By passing the model’s hidden states through its readout, we observed that its diverging dynamics reflected vanishing task information at steady state (Fig. 2b; compare predictions at $t = N$ and $t = T$). These unstable dynamics were not specific to the hGRU. We found similar results for a BPTT-trained convLSTM (Fig. S2), and when optimizing hGRUs with common alternatives to BPTT (Fig. S3).

3 Stabilizing expressive recurrent CNNs

For some applications, RNN performance is not conditional on the stability of their dynamics [41]. However, constraining RNN optimization for non-degenerate and stable dynamics is necessary for utilising constant-memory alternatives to BPTT like RBP, which we expected would improve recurrent CNN performance on large-scale vision challenges. Thus, we designed a “soft” architecture-agnostic constraint for learning local contraction maps, which balances model expressivity and stability over the course of training. Our goal was to derive a constraint to keep the largest singular value of $J_{F,h^*} < 1$, which forces F to be locally contractive at h^* (SI §1.2; this contrasts with the global contraction across dynamics enforced by squashing non-linearities, which is problematic in computer vision as we demonstrate in §2.1). However, the size of this Jacobian is quadratic in hidden

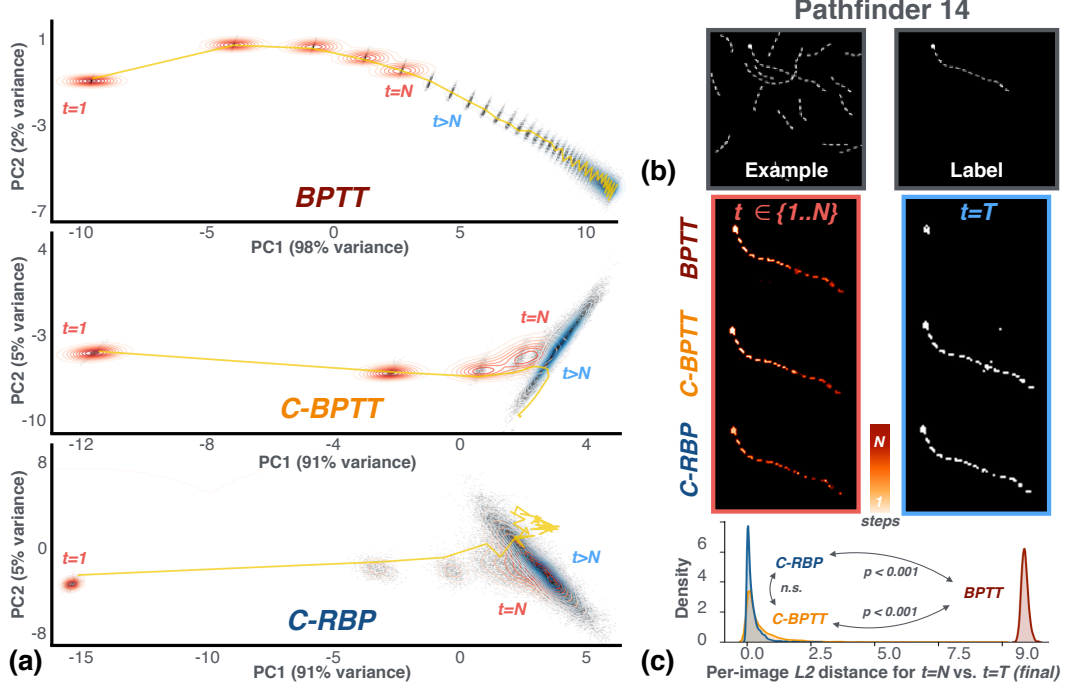


Figure 2: Recurrent CNNs trained with backpropagation through time (BPTT) have unstable dynamics and forget task information. This pathology is corrected by our *Lipschitz Coefficient Penalty* (LCP). (a) Visualization of horizontal gated unit (hGRU) state spaces. Models were trained on Pathfinder-14, and state spaces were visualized by projecting hidden states onto each model’s top-two eigenvectors. Grey dots are the 2D-histogram of projected hidden states, red contours are hidden state densities up to the task-optimized N steps, and blue contours are hidden state densities beyond that point ($t > N$, for 40 steps). Exemplar dynamics for a single image are plotted in yellow. While dynamics of the BPTT-trained model diverge when $t > N$, models trained with LCP did not. We refer to the learning algorithms of LCP-trained models as “contractor-BPTT” (C-BPTT) and “contractor-RBP” (C-RBP). (b) Model dynamics are reflected in their performance on Pathfinder-14. Segmentations evolve over time, as depicted by the colormap. While the BPTT-trained hGRU is accurate at N steps (red box), it fails when asked to process for longer ($t = T = 40$, blue box). (c) Two-sample KS-tests indicate that the distance in state space between $t = N$ and $t = T$ hidden states is significantly greater for an hGRU trained with BPTT than an hGRU trained with C-BPTT or C-RBP (n.s. = not significant).

state dimensions, making it too large to feasibly compute for recurrent CNNs. We overcome this limitation by introducing an approximation, our *Lipschitz Coefficient Penalty* (LCP), which constrains $(\mathbf{1} \cdot J_{F,h^*})_i < \lambda \forall i$, where i is a column index.

$$\|(\mathbf{1} \cdot J_{F,h^*} - \lambda)^+\|_2. \quad (6)$$

Here, $(\cdot)^+$ denotes element-wise rectification and $\lambda \in [0, 1)$ is the hand-selected Lipschitz constant which bounds $\|J_{F,h^*}\|_2$ and hence the degree of contraction in F . The LCP (Eq. 6) can be combined with any task loss for model optimization, and circumvents the need to explicitly determine the Jacobian J_{F,h^*} . We show in SI §1.2 that the vector-Jacobian product used in the LCP, which is efficiently computed through *autograd* in deep learning libraries, serves as an approximate upper bound on the spectral radius of the J_{F,h^*} . Note that because minimizing the LCP implicitly involves the Hessian of F , it is best suited for recurrent CNNs that use activation functions with defined second derivatives (like *softplus* for the hGRU).

3.1 Stable and expressive recurrent CNNs with constant memory complexity

Returning to *Pathfinder*, we tested whether introducing the LCP into training stabilizes the dynamics of models trained with RBP or BPTT. We also tested models on more difficult versions of *Pathfinder* with 14-, 20-, and 25-dash target paths. LCP consists of a single hyperparameter, $\lambda \in [0, 1)$, which mediates the degree of contraction that is imposed. As $\lambda \rightarrow 0^+$, the local contraction at a fixed point

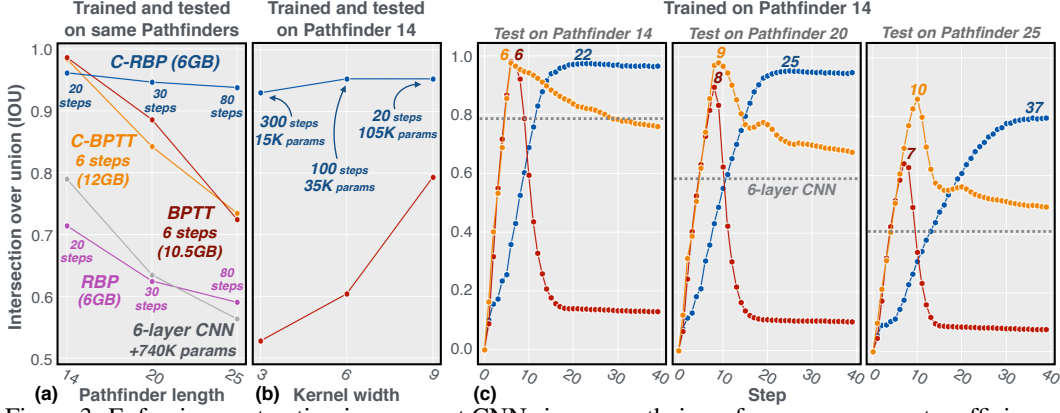


Figure 3: Enforcing contraction in recurrent CNNs improves their performance, parameter efficiency, and enables our constant-memory C-RBP learning algorithm. (a) hGRU models were trained and tested on different versions of *Pathfinder*. Only the version trained with C-RBP, trained for 20 steps, maintained high performance across the three datasets. (b) C-RBP models can rely on recurrent processing rather than spatially broad kernels to solve long-range spatial dependencies. BPTT-trained models cannot practically do this due to their linear memory complexity. (c) LCP improves the stability of hGRU dynamics and, as a result, the generalization of learned visual routines for contour integration. Models were trained on Pathfinder-14, and tested on all three Pathfinder datasets. hGRUs trained with C-RBP and C-BPTT generalized far better than a version trained with BPTT or a 6-layer CNN control. Numbers above each curve denote the max-performing step.

becomes stronger leading to increased stability and reduced expressiveness. In general we find that λ is very dataset dependent, but on *Pathfinder*, models performed well over many settings. We set $\lambda = 0.9$ on the experiments reported here, and adopt the methods described in §2.

Learning a task-optimal trade-off between stability and expressivity. A BPTT-trained hGRU constrained with LCP performed as well as one trained with BPTT with no constraint (0.98 *IoU* for both). However, a state space analysis of this “contractor-BPTT” (C-BPTT) hGRU revealed that it exhibited stable contractor dynamics, unlike the BPTT-trained hGRU (Fig. 2a).

We took this success as evidence that hGRUs trained with LCP satisfy the RBP *constraint qualifications* test. We validated this hypothesis by training a 20-step hGRU with RBP and LCP, which we refer to as “contractor-RBP” (C-RBP). This model nearly as well as both BPTT and C-BPTT trained hGRUs (0.95 *IoU*), despite using approximately half of the memory of either. The C-RBP hGRU also converged to a steady state that maintained task information (Fig. 2b; $t = T$), and like the C-BPTT, the distance between its task-optimized hidden state $t = N$ and steady state $t = T$ was smaller than the BPTT hGRU. Pairwise testing of these distances with 2-sample Kolmogorov–Smirnov (KS) tests revealed that the BPTT hGRU diverged from $t = N$ to $t = T$ significantly more ($\mu = 43.55$, $\sigma = 0.53$, $p < 0.001$) than either C-BPTT or C-RBP hGRUs ($\mu = 1.96$, $\sigma = 2.73$ and $\mu = 0.11$, $\sigma = 0.18$, respectively; Fig. 2c). We repeated these experiments for convLSTMs and found similar results, including C-RBP improving its performance on *Pathfinder* (Fig. S7). C-RBP therefore achieves our main goal of constant-memory training with performance on par with BPTT. However, in the following experiments, we demonstrate several qualities that make C-RBP preferable to BPTT.

C-RBP can solve *Pathfinder* tasks that BPTT cannot. *Pathfinder* difficulty is controlled by increasing the length of the target contour. The recurrent CNNs examined here need more steps of processing to incrementally group target contours as difficulty increases. However, the linear memory complexity of BPTT caps the number of steps that can fit into memory, leading to poor performance on Pathfinder-20 and Pathfinder-25 (Fig. 3a; BPTT and C-BPTT performance). Since C-RBP faces no such memory bottleneck, we were able to train 80-step C-RBP models to solve all versions of *Pathfinder*, achieving > 0.90 *IoU* on each dataset and vastly outperforming other models, including BPTT/RBP-trained hGRUs/convLSTMs, and the 6-layer CNN control model.

C-RBP models can achieve better parameter efficiency through extensive recurrent processing. *Pathfinder* is a test of contour integration, a visual routine for chaining arbitrarily small receptive fields together along the extent of the target contour. The instantaneous receptive field sizes of the recurrent CNNs used here is a function of convolutional kernel sizes. Thus, we hypothesized that

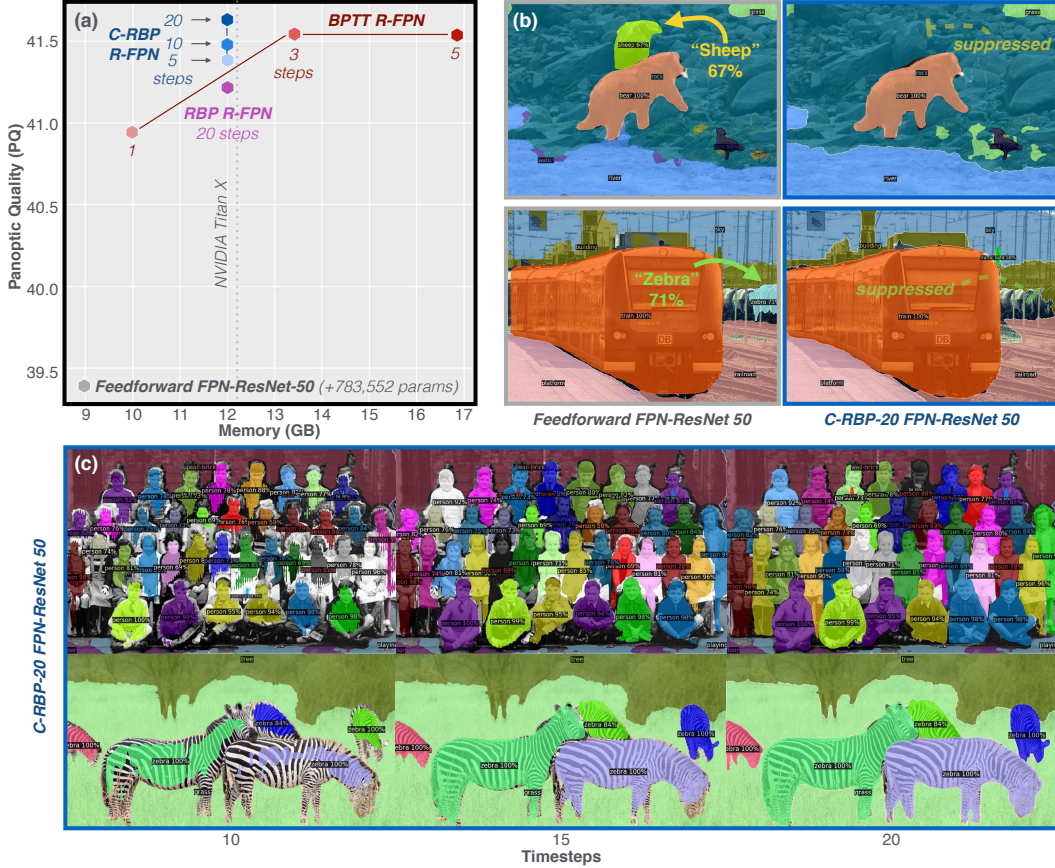


Figure 4: **C-RBP** trained recurrent vision models outperform the feedforward standard on MS-COCO Panoptic Segmentation despite using nearly 800K fewer parameters. (a) Performance of our recurrent FPN-ResNet 50 trained with **C-RBP** improves when trained with more steps of processing, despite remaining constant in its memory footprint. (b) Recurrent processing refines instance segmentations and controls false detections of the standard feedforward architecture (additional examples in SI). (c) Panoptic segmentation timecourses for an FPN-ResNet 50 trained with **C-RBP** for 20 steps.

models with small kernels could solve *Pathfinder* if they had sufficient steps of recurrent processing. Indeed, we found that hGRUs trained with C-RBP for 300 steps but only 3×3 kernels could solve *Pathfinder*-14 nearly as well as the baseline BPTT-trained hGRU with 15×15 kernels (Fig. 3b).

Stable dynamics improve the out-of-distribution generalization of visual routines. Visual routines such as contour integration derive long-range structure from repeated applications of a local grouping rule over steps of processing. This should lead to strong generalization on *Pathfinder*, even when testing out-of-distribution, or between datasets. For instance, increasing target contour length in *Pathfinder* affects the reaction time, but not accuracy, of human observers because they can solve the task through incremental grouping [8, 15]. If recurrent CNNs are learning similarly robust visual routines, a model trained on *Pathfinder*-14 should generalize to *Pathfinder*-20 and *Pathfinder*-25. To test this, we took hGRUs trained with BPTT, C-BPTT, or C-RBP on *Pathfinder*-14, and measured their performance all versions of *Pathfinder* (Fig. 3c). Both C-BPTT and C-RBP trained hGRUs outperformed the BPTT-trained hGRU and feedforward control on each dataset, indicating that the stability exhibited by these models causes their learned visual routines to generalize better. We found a similar improvement for C-RBP trained convLSTMs (Fig. S7). Alternatives to BPTT were not as effective as C-BPTT or C-RBP (Fig. S7).

3.2 Microsoft COCO Panoptic Segmentation

Our main motivation in this paper is to understand – and resolve – the memory bottleneck faced by recurrent CNNs for large-scale computer vision challenges. To date, there have not been competitive recurrent solutions to the MS-COCO Panoptic Segmentation Challenge, a difficult task which involves

recognizing the semantic category and/or object instance occupying every pixel in an image [42]. However, we will show that the stable dynamics and constant memory efficiency of C-RBP allows us to construct recurrent models that outperform the feedforward standards.

Methods The leading approach to Panoptic Segmentation is an FPN Mask-RCNN [42] with a ResNet-50 or ResNet-101 layer backbone (referred to hereafter as FPN-ResNet-50 and FPN-ResNet-101). We developed recurrent extensions of these models, where we replaced the 4-layer Mask-RCNN head with an hGRU containing 3×3 kernels (SI §3.4). We call these models R-FPN-ResNet-50 and R-FPN-ResNet-101. MS-COCO Panoptic Segmentation involves two separate objectives: (i) instance segmentation of the discrete and enumerable “things” in an image, such as people and animals; and (ii) semantic segmentation of the remaining background elements in scenes, or “stuff” as it is known in the challenge. Models were trained to optimize both of these objectives with SGD+Momentum, a learning rate of $5e-2$, and batches of 40 images across 24GB NVIDIA GTX GPUs (10 total). Model predictions on the COCO validation set were scored with Panoptic Quality (PQ), which is the product of metrics for semantic (IoU) and instance (F_1 score) segmentation [42]. Recurrent models trained with LCP used $\lambda = 0.9$; training failed with higher values.

Results After replicating benchmark performance of an FPN-ResNet-50 (39.4PQ, 9GB memory; <https://bit.ly/dtcon>), we evaluated our R-FPN models (Fig. 4a). We first trained versions of the R-FPN-ResNet-50 with BPTT, which used nearly 17GB of memory for 5-steps of processing. BPTT performance increased with recurrence until it plateaued at 3-steps (41.5PQ for both 3- and 5-step models). Next, we trained an R-FPN-ResNet-50 with RBP for 20 steps, and found that this model (41.22PQ, 12GB) performed better than the 1-step R-FPN-ResNet-50, but worse than a 2-step BPTT-trained model (41.45PQ). R-FPN-ResNet-50 models improved when they were trained with C-RBP. A 5-step model trained with C-RBP (41.39, 12GB) outperformed a 20-step model trained with RBP; a 10-step C-RBP model was similar (41.48PQ, 12GB) to the 3- and 5-step BPTT models; and a 20-step C-RBP model performed best (41.63PQ, 12GB). Importantly, each of these R-FPN-ResNet-50 models was more accurate than the feedforward FPN-ResNet-50 despite using 783,552 fewer parameters. We also found that a 20-step C-RBP R-FPN-ResNet-101 outperformed the feedforward FPN-ResNet-101 and BPTT-trained R-FPN-ResNet-101 models (Fig. S9).

The 20-step C-RBP R-FPN-ResNet-50 suppressed false detections of the feedforward model (Fig. 4b, examples of feedforward mistakes, that are corrected by our recurrent model; other examples in Fig. S10-11). It also learned to incrementally segment objects (Fig. 4c), reaching and maintaining steady-state around 20 steps. By contrast, the hidden states of BPTT-trained models lost task information when processing beyond their $t = N$ task-optimized steps (Fig. S8).

3.3 Related work

Memory efficient learning algorithms BPTT’s memory bottleneck has inspired many efficient alternatives. A popular example is truncated back-propagation through time (TBPTT), which improves memory efficiency by utilizing a shorter time horizon for credit assignment. There are also heuristics for overcoming the BPTT memory bottleneck by swapping memory between GPU and CPU during training [43, 44], or “gradient checkpointing”, and recomputing a number of intermediate activities during the backwards pass [45–47]. Neural ODEs can train neural networks with continuous-time dynamics by optimizing through black box ODE solvers, but their computational demands and numerical issues have yielded poor performance on vision tasks ([48, 48], see SI §4.1 for an expanded discussion). Deep equilibrium models (DEQ) are another constant-memory complexity learning algorithm with good performance on sequence modeling, rivaling the state of the art [28]. However, we found that training recurrent CNNs with DEQ is unstable, like we observed with RBP (SI §4.1).

Stable RNNs Recurrent model “stability” is typically analyzed w.r.t. training, where exploding or vanishing gradients are a byproduct of gradient descent [41, 49]. Models are stable if their Jacobians are upper-bounded by λ (i.e., it is λ -contractive). One way to achieve this is with architecture-specific constraints on model parameters, which has worked well for generative adversarial networks (GANs) [50, 51] and sequence modeling LSTMs [41]. A simple alternative, is to directly penalize Jacobian approximations, as has been done for GANs [52–54]. However, these approximations have not been investigated for recurrent vision models or in the context of visual recognition.

4 Conclusion

There is compelling evidence from biological and artificial vision on the importance of recurrent processing for the visual routines which support robust perception [2, 5, 17]. Until now, the enormous cost of training recurrent CNNs with BPTT has made it difficult to test whether recurrence can translate into improvements on large-scale computer vision challenges, which are dominated by high-capacity feedforward CNNs. C-RBP alleviates this bottleneck, enabling constant-memory recurrent dynamics, more parameter efficient architectures, and better generalization. Our findings are relevant to any domain in which recurrent models can be sensibly applied, and we release all code and data to support these applications.

Acknowledgments and Disclosure of Funding

We are grateful to Alexander Fengler, Remi Cadene, Mathieu Chalvidal, Andrea Alamia, and Amir Soltani for their feedback on the manuscript. This work was funded by ONR grant #N00014-19-1-2029 and the ANR-3IA Artificial and Natural Intelligence Toulouse Institute. Additional support provided by the Carney Institute for Brain Science and the Initiative for Computation in Brain and Mind at Brown University and the Center for Computation and Visualization (CCV). TS serves as a scientific advisor for Vium Inc, which may potentially benefit from the research results.

References

- [1] Gilbert, C.D., Li, W.: Top-down influences on visual processing. *Nat. Rev. Neurosci.* **14**(5) (May 2013) 350–363
- [2] Ullman, S.: Visual routines. *Cognition* **18**(1-3) (December 1984) 97–159
- [3] Roelfsema, P.R.: Cortical algorithms for perceptual grouping. *Annu. Rev. Neurosci.* **29** (January 2006) 203–227
- [4] DiCarlo, J.J., Cox, D.D.: Untangling invariant object recognition. *Trends Cogn. Sci.* **11**(8) (August 2007) 333–341
- [5] Roelfsema, P.R., Lamme, V.A., Spekreijse, H.: The implementation of visual routines. *Vision Res.* **40**(10-12) (2000) 1385–1411
- [6] Kreiman, G., Serre, T.: Beyond the feedforward sweep: feedback computations in the visual cortex. *Ann. N. Y. Acad. Sci.* **1464**(1) (March 2020) 222–241
- [7] Linsley, D., Kim, J., Veerabadran, V., Serre, T.: Learning long-range spatial dependencies with horizontal gated-recurrent units. (May 2018)
- [8] Kim*, J., Linsley*, D., Thakkar, K., Serre, T.: Disentangling neural mechanisms for perceptual grouping. *International Conference on Representation Learning* (2020)
- [9] Liang, M., Hu, X.: Recurrent convolutional neural network for object recognition. In: 2015 IEEE Conference on Computer Vision and Pattern Recognition (CVPR), IEEE Computer Society (June 2015) 3367–3375
- [10] Kim, J., Lee, J.K., Lee, K.M.: Deeply-Recursive convolutional network for image Super-Resolution. In: 2016 IEEE Conference on Computer Vision and Pattern Recognition (CVPR), IEEE (June 2016) 1637–1645
- [11] Li, R., Li, K., Kuo, Y., Shu, M., Qi, X., Shen, X., Jia, J.: Referring image segmentation via recurrent refinement networks. In: 2018 IEEE/CVF Conference on Computer Vision and Pattern Recognition. (June 2018) 5745–5753
- [12] Linsley, D., Kim, J., Veerabadran, V., Windolf, C., Serre, T.: Learning long-range spatial dependencies with horizontal gated recurrent units. In Bengio, S., Wallach, H., Larochelle, H., Grauman, K., Cesa-Bianchi, N., Garnett, R., eds.: *Advances in Neural Information Processing Systems* 31. Curran Associates, Inc. (2018) 152–164
- [13] Tang, H., Schrimpf, M., Lotter, W., Moerman, C., Paredes, A., Ortega Caro, J., Hardesty, W., Cox, D., Kreiman, G.: Recurrent computations for visual pattern completion. *Proc. Natl. Acad. Sci. U. S. A.* **115**(35) (August 2018) 8835–8840

- [14] Lotter, W., Kreiman, G., Cox, D.: Deep predictive coding networks for video prediction and unsupervised learning. (May 2016)
- [15] Houtkamp, R., Roelfsema, P.R.: Parallel and serial grouping of image elements in visual perception. *J. Exp. Psychol. Hum. Percept. Perform.* **36**(6) (December 2010) 1443–1459
- [16] Linsley, D., Kim, J., Berson, D., Serre, T.: Robust neural circuit reconstruction from serial electron microscopy with convolutional recurrent networks. (November 2018)
- [17] Linsley, D., Kim, J., Ashok, A., Serre, T.: Recurrent neural circuits for contour detection. *International Conference on Learning Representations* (2020)
- [18] Kubilius, J., Schrimpf, M., Nayebi, A., Bear, D., Yamins, D.L.K., DiCarlo, J.J.: CORnet: Modeling the neural mechanisms of core object recognition. (September 2018)
- [19] Kubilius, J., Schrimpf, M., Kar, K., Rajalingham, R., Hong, H., Majaj, N., Issa, E., Bashivan, P., Prescott-Roy, J., Schmidt, K., Nayebi, A., Bear, D., Yamins, D.L., DiCarlo, J.J.: Brain-Like object recognition with High-Performing shallow recurrent ANNs. In Wallach, H., Larochelle, H., Beygelzimer, A., d Alché-Buc, F., Fox, E., Garnett, R., eds.: *Advances in Neural Information Processing Systems 32*. Curran Associates, Inc. (2019) 12805–12816
- [20] Nayebi, A., Bear, D., Kubilius, J., Kar, K., Ganguli, S., Sussillo, D., DiCarlo, J.J., Yamins, D.: Task-Driven convolutional recurrent models of the visual system. In: *Neural Information Processing Systems*. (2018)
- [21] Kar, K., Kubilius, J., Schmidt, K., Issa, E.B., DiCarlo, J.J.: Evidence that recurrent circuits are critical to the ventral stream’s execution of core object recognition behavior. *Nat. Neurosci.* (April 2019)
- [22] Sinz, F., Ecker, A.S., Fahey, P., Walker, E., others: Stimulus domain transfer in recurrent models for large scale cortical population prediction on video. *Adv. Neural Inf. Process. Syst.* (2018)
- [23] Kietzmann, T.C., Spoerer, C.J., Sörensen, L., others: Recurrence required to capture the dynamic computations of the human ventral visual stream. *arXiv preprint arXiv* (2019)
- [24] Lin, T.Y., Maire, M., Belongie, S., Bourdev, L., Girshick, R., Hays, J., Perona, P., Ramanan, D., Lawrence Zitnick, C., Dollár, P.: Microsoft COCO: Common objects in context. (May 2014)
- [25] Werbos, P.J.: Backpropagation through time: what it does and how to do it. *Proc. IEEE* **78**(10) (October 1990) 1550–1560
- [26] Tan, M., Le, Q.V.: EfficientNet: Rethinking model scaling for convolutional neural networks. (May 2019)
- [27] Liao, R., Xiong, Y., Fetaya, E., Zhang, L., Yoon, K., Pitkow, X., Urtasun, R., Zemel, R.: Reviving and improving recurrent Back-Propagation. (March 2018)
- [28] Bai, S., Kolter, J.Z., Koltun, V.: Deep equilibrium models. In: *Advances in Neural Information Processing Systems (NeurIPS)*. (2019)
- [29] Almeida, L.B.: A learning rule for asynchronous perceptrons with feedback in a combinatorial environment. In Caudil, M., Butler, C., eds.: *Proceedings of the IEEE First International Conference on Neural Networks San Diego, CA*. (1987) 609–618
- [30] Pineda, F.J.: Generalization of back-propagation to recurrent neural networks. *Phys. Rev. Lett.* **59**(19) (November 1987) 2229–2232
- [31] Hopfield, J.J.: Neural networks and physical systems with emergent collective computational abilities. *Proc. Natl. Acad. Sci. U. S. A.* **79**(8) (April 1982) 2554–2558
- [32] Rudin, W.: *Principles of mathematical analysis*. Volume 3. McGraw-Hill New York (1964)
- [33] Scarselli, F., Gori, M., Tsoi, A.C., Hagenbuchner, M., Monfardini, G.: The graph neural network model. *IEEE Trans. Neural Netw.* **20**(1) (January 2009) 61–80
- [34] Linsley, D., Shiebler, D., Eberhardt, S., Serre, T.: Learning what and where to attend. In: *International Conference on Learning Representations*. (2019)
- [35] Ioffe, S., Szegedy, C.: Batch normalization: accelerating deep network training by reducing internal covariate shift. In: *Proceedings of the 32nd International Conference on International Conference on Machine Learning - Volume 37, JMLR.org* (July 2015) 448–456
- [36] Kingma, D.P., Ba, J.: Adam: A method for stochastic optimization. (December 2014)

- [37] Glorot, X., Bordes, A., Bengio, Y.: Deep sparse rectifier neural networks. In Gordon, G., Dunson, D., Dudík, M., eds.: *Proceedings of the Fourteenth International Conference on Artificial Intelligence and Statistics*. Volume 15 of *Proceedings of Machine Learning Research*, Fort Lauderdale, FL, USA, PMLR (2011) 315–323
- [38] Glorot, X., Bengio, Y.: Understanding the difficulty of training deep feedforward neural networks. In Teh, Y.W., Titterton, M., eds.: *Proceedings of the Thirteenth International Conference on Artificial Intelligence and Statistics*. Volume 9 of *Proceedings of Machine Learning Research*, Chia Laguna Resort, Sardinia, Italy, PMLR (2010) 249–256
- [39] Gulcehre, C., Moczulski, M., Denil, M., Bengio, Y.: Noisy activation functions. In: *Proceedings of the 33rd International Conference on International Conference on Machine Learning - Volume 48*. ICML’16, JMLR.org (June 2016) 3059–3068
- [40] Clevert, D.A., Unterthiner, T., Hochreiter, S.: Fast and accurate deep network learning by exponential linear units (ELUs). *International Conference on Learning Representations* (November 2015)
- [41] Miller, J., Hardt, M.: Stable recurrent models. *International Conference on Representation Learning (ICLR)* (September 2018)
- [42] Kirillov, A., He, K., Girshick, R., Rother, C., Dollár, P.: Panoptic segmentation. In: *2019 IEEE/CVF Conference on Computer Vision and Pattern Recognition (CVPR)*. (June 2019) 9396–9405
- [43] Dean, J., Corrado, G., Monga, R., Chen, K., Devin, M., Mao, M., aurelio Ranzato, M., Senior, A., Tucker, P., Yang, K., Le, Q.V., Ng, A.Y.: Large scale distributed deep networks. In Pereira, F., Burges, C.J.C., Bottou, L., Weinberger, K.Q., eds.: *Advances in Neural Information Processing Systems 25*. Curran Associates, Inc. (2012) 1223–1231
- [44] Rhu, M., Gimelshein, N., Clemons, J., Zulfiqar, A., Keckler, S.W.: vDNN: virtualized deep neural networks for scalable, memory-efficient neural network design. In: *The 49th Annual IEEE/ACM International Symposium on Microarchitecture*. Number Article 18 in MICRO-49, IEEE Press (October 2016) 1–13
- [45] Dauvergne, B., Hascoët, L.: The Data-Flow equations of checkpointing in reverse automatic differentiation. In: *Computational Science – ICCS 2006*, Springer Berlin Heidelberg (2006) 566–573
- [46] Chen, J., Yang, L., Zhang, Y., Alber, M., Chen, D.Z.: Combining fully convolutional and recurrent neural networks for 3D biomedical image segmentation. In Lee, D.D., Sugiyama, M., Luxburg, U.V., Guyon, I., Garnett, R., eds.: *Advances in Neural Information Processing Systems 29*. Curran Associates, Inc. (2016) 3036–3044
- [47] Gruslys, A., Munos, R., Danihelka, I., Lanctot, M., Graves, A.: Memory-efficient backpropagation through time. In: *Proceedings of the 30th International Conference on Neural Information Processing Systems*. NIPS’16, Red Hook, NY, USA, Curran Associates Inc. (December 2016) 4132–4140
- [48] Dupont, E., Doucet, A., Teh, Y.W.: Augmented neural ODEs. In Wallach, H., Larochelle, H., Beygelzimer, A., d Alché-Buc, F., Fox, E., Garnett, R., eds.: *Advances in Neural Information Processing Systems 32*. Curran Associates, Inc. (2019) 3140–3150
- [49] Bengio, Y., Simard, P., Frasconi, P.: Learning long-term dependencies with gradient descent is difficult. *IEEE Trans. Neural Netw.* **5**(2) (1994) 157–166
- [50] Yoshida, Y., Miyato, T.: Spectral norm regularization for improving the generalizability of deep learning. *arXiv preprint arXiv:1705.10941* (2017)
- [51] Miyato, T., Kataoka, T., Koyama, M., Yoshida, Y.: Spectral normalization for generative adversarial networks. *International Conference on Learning Representations* (2018)
- [52] Gu, S., Rigazio, L.: Towards deep neural network architectures robust to adversarial examples. (December 2014)
- [53] Gulrajani, I., Ahmed, F., Arjovsky, M., Dumoulin, V., Courville, A.: Improved training of wasserstein GANs. In: *Proceedings of the 31st International Conference on Neural Information Processing Systems*. NIPS’17, Red Hook, NY, USA, Curran Associates Inc. (December 2017) 5769–5779

- [54] Wei, X., Gong, B., Liu, Z., Lu, W., Wang, L.: Improving the improved training of wasserstein GANs: A consistency term and its dual effect. *International Conference on Learning Representations* (March 2018)
- [55] Cooijmans, T., Ballas, N., Laurent, C., Gülçehre, Ç., Courville, A.: Recurrent batch normalization. In: *International Conference on Learning Representations*. (2017)
- [56] Maheswaranathan, N., Williams, A., Golub, M.D., Ganguli, S., Sussillo, D.: Reverse engineering recurrent networks for sentiment classification reveals line attractor dynamics. (June 2019)
- [57] Lin, T., Dollár, P., Girshick, R., He, K., Hariharan, B., Belongie, S.: Feature pyramid networks for object detection. In: *2017 IEEE Conference on Computer Vision and Pattern Recognition (CVPR)*. (July 2017) 936–944
- [58] Wu, Y., He, K.: Group normalization. (March 2018)
- [59] George, D., Lechach, W., Kansky, K., Lázaro-Gredilla, M., Laan, C., Marthi, B., Lou, X., Meng, Z., Liu, Y., Wang, H., Lavin, A., Phoenix, D.S.: A generative vision model that trains with high data efficiency and breaks text-based CAPTCHAs. *Science* **358**(6368) (December 2017)
- [60] Spoerer, C.J., McClure, P., Kriegeskorte, N.: Recurrent convolutional neural networks: A better model of biological object recognition. *Front. Psychol.* **8** (September 2017) 1551
- [61] Zamir, A.R., Wu, T.L., Sun, L., Shen, W., Malik, J., Savarese, S.: Feedback networks. (December 2016)
- [62] Wen, H., Han, K., Shi, J., Zhang, Y., Culurciello, E., Liu, Z.: Deep predictive coding network for object recognition. (February 2018)
- [63] Liao, Q., Poggio, T.: Bridging the gaps between residual learning, recurrent neural networks and visual cortex. (April 2016)
- [64] Rifai, S., Vincent, P., Muller, X., Glorot, X., Bengio, Y.: Contractive auto-encoders: explicit invariance during feature extraction. In: *Proceedings of the 28th International Conference on International Conference on Machine Learning. ICML’11, Madison, WI, USA, Omnipress* (June 2011) 833–840
- [65] Hochreiter, S., Schmidhuber, J.: Long short-term memory. *Neural Comput.* **9**(8) (November 1997) 1735–1780
- [66] Simard, P.Y., Ottaway, M.B., Ballard, D.H.: Fixed point analysis for recurrent networks. In Touretzky, D.S., ed.: *Advances in Neural Information Processing Systems 1*. Morgan-Kaufmann (1989) 149–159
- [67] Zhang, J., Lei, Q., Dhillon, I.S.: Stabilizing gradients for deep neural networks via efficient SVD parameterization. (March 2018)
- [68] Chen, W., Zhang, Y., He, J., Qiao, Y., Chen, Y., Shi, H., Tang, X.: Prostate segmentation using 2D bridged u-net. (July 2018)

A Extended background

A.1 Backpropagation through time (BPTT)

BPTT is the standard learning algorithm for optimizing recurrent parameters w_F w.r.t. a loss $\mathcal{L}(\tilde{y}, y)$. It is implemented by replicating a dynamical system and accumulating its gradients over N steps of processing (Eq. 7, $K = 0$). Given a recurrent function F parameterized by w_F , which maintains a latent state h_t for each time step t , BPTT is implemented by Eq. 7.

$$\frac{\partial \mathcal{L}}{\partial w_F} = \frac{\partial \mathcal{L}}{\partial \tilde{y}} \frac{\partial \tilde{y}}{\partial h_T} \sum_{k=K}^{k=T-1} \left(\prod_{i=T}^{i=T-k} J_F(h_i) \right) \frac{\partial F}{\partial w_F}(x, h_{T-k}, w_F). \quad (7)$$

Note that this algorithm stores every h_t in memory during the forward pass, causing a memory footprint that linearly increases with steps.

A.2 Lipschitz Coefficient Penalty

We designed the *Lipschitz Coefficient Penalty* (LCP) as a hyperparameter-agnostic regularization for forcing recurrent CNNs to learn contraction maps. As mentioned in the main text, LCP constrains $(\mathbf{1} \cdot J_{F,h^*})_i < 1 \ \forall i$, where i is a column index.

$$\|(\mathbf{1} \cdot J_{F,h^*} - \lambda)^+\|_2. \quad (8)$$

where, $(\cdot)^+$ denotes element-wise rectification and $\lambda \in [0, 1]$ controls the degree of contraction in F . To derive LCP, we begin from the first-order Taylor expansion of $F(h)$,

$$F(h) \approx F(\bar{h}) + J_{F,\bar{h}} \cdot (h - \bar{h}) + \dots,$$

With which one can show:

$$\frac{\|F(h) - F(\bar{h})\|_2}{\|h - \bar{h}\|_2} \approx \frac{\|J_{F,\bar{h}} \cdot (h - \bar{h})\|_2}{\|h - \bar{h}\|_2}, \quad (9)$$

Recalling the necessary condition for F being a contractive map,

$$\|F(h) - F(\bar{h})\|_2 < \lambda \|h - \bar{h}\|_2, \quad (10)$$

we can observe that the right hand side of Eq. 9 must be less than or equal to $\lambda \in [0, 1]$ for any h sufficiently close to \bar{h} . Thus, $F(\cdot)$ will be λ -contractive *at least in the neighbourhood of \bar{h}* if the LHS is forced to be less than λ . We accomplish this goal by explicitly regularizing $\bar{h} = h^*$ over the course of training:

$$\|J_{F,h^*} \cdot \hat{v}\|_2 < 1, \quad (11)$$

for all unit vectors \hat{v} , which implies that the largest singular value of J_{F,h^*} must be less than 1. This is equivalent to requiring $\|J_{F,h^*}\|_2 < 1$. Note that $\|h - h^*\|_2$ may not necessarily be small for all h 's sampled along our trajectories, and so the Taylor approximation and hence Eq. (9) may not hold. Nevertheless, in experiments on Pathfinder and Microsoft COCO our regularisation still yields reasonably stable convergence to fixed points.

Indeed, the matrix 2-norm is bounded from above and below by the 1-norm,

$$1/\sqrt{n} \|J_{F,h^*}\|_1 \leq \|J_{F,h^*}\|_2 \leq \sqrt{n} \|J_{F,h^*}\|_1, \quad (12)$$

where

$$\|J_{F,h^*}\|_1 = \max_i \sum_j |(J_{F,h^*})_{ij}|. \quad (13)$$

and n is the dimensionality of the Jacobian matrix. So if we can regularise our loss by forcing $\sqrt{n} \|J_{F,h^*}\|_1$ to be below 1, then we can ensure that $F(\cdot)$ will be contractive. However, computing Jacobians of large matrices requires an enormous memory load, and it is far more efficient to compute vector-Jacobian products instead. We shall instead approximate the 1-norm by taking

$$\max_i \left| \sum_j (J_{F,h^*})_{ij} \right| = \max_i (\mathbf{1} \cdot J_{F,h^*})_i, \quad (14)$$

where $\mathbf{1}$ denotes the row vector with all entries being 1. We note that in using this approximation, the right inequality in (12) ceases to be a strict upper bound, but we find that the approximation works well in practice due to large n .

We regularise model training with this approximation by requiring that $(\mathbf{1} \cdot J_{F,h^*})_i < 1 \ \forall i$. This yields our *Lipschitz Coefficient Penalty* (LCP):

$$\|(\mathbf{1} \cdot J_{F,h^*} - \lambda)^+\|_2, \quad (15)$$

which can be added to any task loss. Here, $(\cdot)^+$ denotes element-wise rectification and $\lambda \in [0, 1]$ is a hand-selected constant controlling the bound on $\|J_{F,h^*}\|_2$ and hence the degree of contraction in F .

B Recurrent Back-prop

We review the Recurrent Back-Prop (RBP) learning algorithm of [29, 30]. Given a transition function F , which is parameterized by w_F and applied to the static drive x , hidden state h over $t \in \{1..N\}$ steps of processing: $h_{t+1} = F(x, h_t, w_F)$. We define a model readout, $\tilde{y} = G(h_T, w_G)$, where G is a task-optimized readout parameterized by w_G . We also introduce a loss \mathcal{L} which yields a distance between predicted and ground-truth outputs. By differentiating the loss with respect to the weights, we obtain the gradients:

$$\frac{\partial \mathcal{L}_\infty}{\partial w_G} = \frac{\partial \mathcal{L}_\infty}{\partial y_\infty} \frac{\partial G(x; h^*, w_G)}{\partial w_G}, \quad (16)$$

$$\frac{\partial \mathcal{L}_\infty}{\partial w_F} = \frac{\partial \mathcal{L}_\infty}{\partial y_\infty} \frac{\partial y_\infty}{\partial h^*} \frac{\partial h^*}{\partial w_F}. \quad (17)$$

To obtain an expression for $\partial h^* / \partial w_F$, we first introduce the auxiliary function

$$\Psi(w_F, h) = h - F(x, h, w_F), \quad (18)$$

where, at a fixed point, $\Psi(w_F, h^*) = 0$. Differentiating with respect to w_F , we obtain

$$\begin{aligned} \frac{\partial \Psi(w_F, h^*)}{\partial w_F} &= \frac{\partial h^*}{\partial w_F} - \frac{dF(x, h^*, w_F)}{dw_F} \\ &= \left(I - \frac{\partial F(x, h^*, w_F)}{\partial h^*} \right) \frac{\partial h^*}{\partial w_F} - \frac{\partial F(x, h^*, w_F)}{\partial w_F} \\ &= 0. \end{aligned}$$

Rearranging yields

$$\frac{\partial h^*}{\partial w_F} = (I - J_{F,h^*})^{-1} \frac{\partial F(x, h^*, w_F)}{\partial w_F}, \quad (19)$$

where J_{F,h^*} is the Jacobian matrix $\partial F(x, h^*, w_F) / \partial h^*$. The implicit function theorem guarantees the existence and uniqueness of a function mapping w_F to h^* and hence of $\partial h^* / \partial w_F$ provided (i) $\Psi(w_F, h)$ is continuously differentiable and (ii) $(I - J_{F,h^*})$ is invertible. The main virtue of RBP is that the memory it requires to train the RNN is constant with respect to the granularity of dynamics (steps of processing).

C Recurrent vision models

C.1 Pathfinder

Horizontal Gated Recurrent Units The hGRU is recurrent CNN, which when placed on top of a conventional feedforward convolutional layer, implements long-range nonlinear interactions between the feedforward layer’s units [7]. These interactions take place over “horizontal connections” – a concept from neuroscience, in which anatomical connections between nearby cortical neurons (in retinotopic space) are the substrate for complex recurrent processing. Tracing back to its origins as a neural circuit model, the hGRU distinguishes itself from other recurrent CNNs as having two distinct stages of processing with independent kernels in each. The first stage is used for computing suppressive interactions, i.e., a unit at location (x, y) inhibits activity in a unit at location $(x + n, y)$, where n is a spatial offset between these units. The second stage is used for computing facilitative

interactions, i.e., a unit (x, y) excites activity in a unit at location $(x, y + n)$. The hGRU is governed by the following equations:

Stage 1:

$$\begin{aligned}
\mathbf{A}^S &= U^S * \mathbf{H}[t-1] && \# \text{ Compute channel-wise selection} \\
\mathbf{G}^S &= \text{sigmoid}(\mathbf{A}^S) && \# \text{ Compute suppression gate} \\
\mathbf{C}^S &= \text{BN}(W^S * (\mathbf{H}[t-1] \odot \mathbf{G}^S)) && \# \text{ Compute suppression interactions} \\
\mathbf{S} &= \left[\mathbf{Z} - \left[(\alpha \mathbf{H}[t-1] + \mu) \mathbf{C}^S \right]_+ \right]_+, && \# \text{ Additive and multiplicative suppression of } \mathbf{Z}
\end{aligned}$$

Stage 2:

$$\begin{aligned}
\mathbf{G}^F &= \text{sigmoid}(U^F * \mathbf{S}) && \# \text{ Compute channel-wise recurrent updates} \\
\mathbf{C}^F &= \text{BN}(W^F * \mathbf{S}) && \# \text{ Compute facilitation interactions} \\
\tilde{\mathbf{H}} &= \left[\nu(\mathbf{C}^F + \mathbf{S}) + \omega(\mathbf{C}^F * \mathbf{S}) \right]_+ && \# \text{ Additive and multiplicative facilitation of } \mathbf{S} \\
\mathbf{H}[t] &= (1 - \mathbf{G}^F) \odot \mathbf{H}[t-1] + \mathbf{G}^F \odot \tilde{\mathbf{H}} && \# \text{ Update recurrent state}
\end{aligned}$$

$$\text{where } \text{BN}(\mathbf{R}; \delta, \nu) = \nu + \delta \odot \frac{\mathbf{R} - \widehat{\mathbb{E}}[\mathbf{R}]}{\sqrt{\widehat{\text{Var}}[\mathbf{R}] + \eta}}.$$

Here, $\mathbf{H}, \mathbf{Z} \in \mathcal{R}^{X \times Y \times C}$ are the hidden state and static drive from a preceding convolutional layer, respectively, with height/width/channels X, Y, C . Suppressive interactions in Stage 1 are computed with $W^S \in \mathbb{R}^{E \times E \times C \times C}$, and facilitative interactions in Stage 2 are computed with $W^F \in \mathbb{R}^{E \times E \times C \times C}$, where E is the spatial extent of the horizontal connection kernel. In most of our experiments we set $E = 15$, as in [7] (other kernel sizes were tested in our parameter efficiency analysis in Fig. 3b). The hGRU also contains gates to modulate input activity and interpolate the previous hidden state with the current step's state, $U^S, U^F \in \mathbb{R}^{1 \times 1 \times C \times C}$. Steps of processing are indexed by $t \in \{1..N\}$, and rectification using *softplus* pointwise nonlinearities is denoted by $[\cdot]_+$, which ensures non-negativity in each stage, and hence, guarantees on suppression vs. facilitation. Lastly, we use batch normalization in the module to control exploding/vanishing gradients [55]. This introduces two learned kernels, $\delta, \nu \in \mathbb{R}^{1 \times 1 \times C}$, which control the scale and bias of normalization over input feature maps \mathbf{R} , and are shared across steps of processing (η is a small constant that protects divide-by-zero errors). As is standard in batch normalization, $\widehat{\mathbb{E}}$ and $\widehat{\text{Var}}$ are estimated on-line during training.

Convolution LSTM We use a standard implementation of convolutional LSTMs from [14]. These models used kernels with the same dimensions as those described above for the hGRU.

C.2 State space analysis

We analyzed the state space of recurrent models trained to solve *Pathfinder*. This classic technique from dynamical systems has shown promise for analyzing computations of task-optimized recurrent neural networks [56]. Our approach to visualizing model state spaces involved the following steps: **(i)** Extract model hidden states for steps $t \in \{1..T\}$ elicited by a Pathfinder-14 image. **(ii)** Reduce hidden state dimensionality with a global average pool across spatial dimensions, yielding C -dimensional vectors. **(iii)** Fit a PCA using the $t \in \{1..N\}$ task-optimized steps of processing. **(iv)** Project all $t \in \{1..T\}$ hidden states onto the extracted eigenvectors.

C.3 Panoptic Segmentation

As a proof-of-concept of C-RBP on large-scale computer vision challenges, we developed a straightforward recurrent extension to the leading feedforward approach to the MSCOCO Panoptic Segmentation challenge: the FPN-ResNet. This model uses a ResNet backbone (either 50- or 101-layers) pretrained on ImageNet, which passes its activities to a feature pyramid network (FPN; [57]). FPN activities are then sent to a linear readout for semantic segmentation (to identify the “stuff” in images) and a

Mask-RCNN for instance segmentation (to identify and individuate the “things”). We replace the Mask-RCNN head, which consists of 4-layers of convolutions and linear rectifications, with a single hGRU module (for both our version and the standard, activities from this stage are next upsampled, rectified, and linearly transformed into predictions). The hGRU that we used is slightly different than the one for the *Pathfinder* challenge above. Batch normalization was replaced with group normalization [58], which is standard for Panoptic segmentation. We also used a modification of the input gate, following [17], which was found to improve performance for natural image processing. Standard feedforward FPN-ResNets were approximately twice as fast to train as our 20-step C-RBP R-FPN-ResNets. Models with ResNet-50 backbones took between one and two days to train, whereas models with ResNet-101 backbones took two and four days to train.

D Extended discussion

D.1 Related work

Recurrent vision models There are many successful applications of recurrent CNNs in computer vision, including object recognition, segmentation, and super-resolution tasks [9–14, 59]. These models often augment popular feedforward CNN architectures with local (within a layer) and/or long-range (between-layer) recurrent connections.

Others have found that augmenting recurrent CNNs with connectivity patterns or objective functions that are inspired by the anatomy or the physiology of the visual cortex can improve performance in visual reasoning, prediction, and recognition of occluded objects [12–14, 59–63].

Lipschitz constraints for stable training There are many examples of using constraints on Lipschitz continuity to stabilize deep network training. This is especially popular for generative adversarial networks (GANs), where stability is enhanced by constraining the spectral norm of the weights [50, 51], or Jacobians of each layer of the discriminator [52], or through Monte Carlo estimation of the discriminator’s Jacobian [53, 54]. Penalizing the spectral norm of Jacobians can also yield better Auto Encoders [64], and adversarial robustness in CNNs [52]. In contrast to prior works on penalizing network Jacobians, in the current work we describe (i) an application to recurrent vision models, which (ii) enforces contractions only locally around equilibrium points (rather than globally across a hierarchy), which is a weaker constraint on model expressivity that still supports our key goal of stability during inference.

RNNs are notoriously challenging to train [49], and the classic solution is to constrain Lipschitz continuity by introducing learnable gates [41, 65]. It should be emphasized that our models also take advantage of gates, and while these control vanishing and exploding gradients to stabilize training, they are not sufficient to yield contractive mappings. More generally, it has been found that stability is critical to train RNNs that can solve sequence modeling tasks [66], but that stability is less critical for BPTT [41]. Other recent approaches induce stability via other architectural constraints, like weight orthogonalization via SVD [67].

Deep networks as ODEs Neural ODEs exploit the observation that the residual networks can be treated as a discrete-time ODE. By using black-box ODE solvers in the forward and backward passes of the network, this discretization can be taken towards zero [68]. These models are trained with back-propagation through a latent trajectory derived from an adjoint system, giving them constant memory efficiency w.r.t. the granularity of dynamics, and they have shown promise in modeling continuous-time data and normalizing flows. However, Neural ODEs face several issues for computer vision applications. (i) Neural ODEs are difficult to optimize because input-output mappings become arbitrarily complex over the course of training. (ii) The adjoint method is slow to compute. (iii) Neural ODEs require feature engineering to fit certain classes of non-linear data manifolds [48], and (iv) they (along with the recent Augmented Neural ODEs [48]) do not compare favorably to standard feedforward models on simple computer vision benchmarks like CIFAR.

Deep Equilibrium Models A recent extension to RBP includes a Neumann-series computation to approximate the inverse of a dynamical system’s Jacobian [27]. Separately, deep equilibrium models (DEQ) use root-finding algorithms to exploit an identical formulation as in Eq. 3 to compute the steady state h^* [28]. Both RBP and DEQ algorithms are effective for sequence modeling and

meta-learning tasks, but have yet to be extended to vision. We attempted to train our hGRU models on Pathfinder 14 with DEQ, but it performed as poorly as the RBP-trained model, while using more GPU memory and taking longer to train.

D.2 Future directions and limitation

Our work is a successful proof of concept for C-RBP in tightly controlled computer vision experiments and large-scale computer vision challenges. However, the scope of our experiments leave several open questions about the effectiveness of C-RBP on certain types of dynamics, architectures, and computer vision domains.

- It is unclear whether C-RBP can extend to complex dynamical systems with limit cycles or strange attractors. Additional experiments and potentially extensions are needed to transform C-RBP into a general method for optimizing recurrent neural networks to explain arbitrary dynamical systems.
- It is unclear whether our approach extends to complex recursive architectures where all recurrent layers are on the same dynamic “clock”, such as is the case with the recent γ -net of [17]. Applying C-RBP to these types of architectures will be especially impactful for computational neuroscience, where it was found that optimizing a γ -net for a dense prediction task yielded human-like visual illusions in the model which were absent from purely feedforward models.
- It is likely that our C-RBP formulation will need adjustments to optimally extend to model spatiotemporal tasks in computer vision, like action recognition and tracking. This is because recurrent neural networks applied to spatiotemporal processing have a time-varying drive, unlike the static image processing setting investigated here.

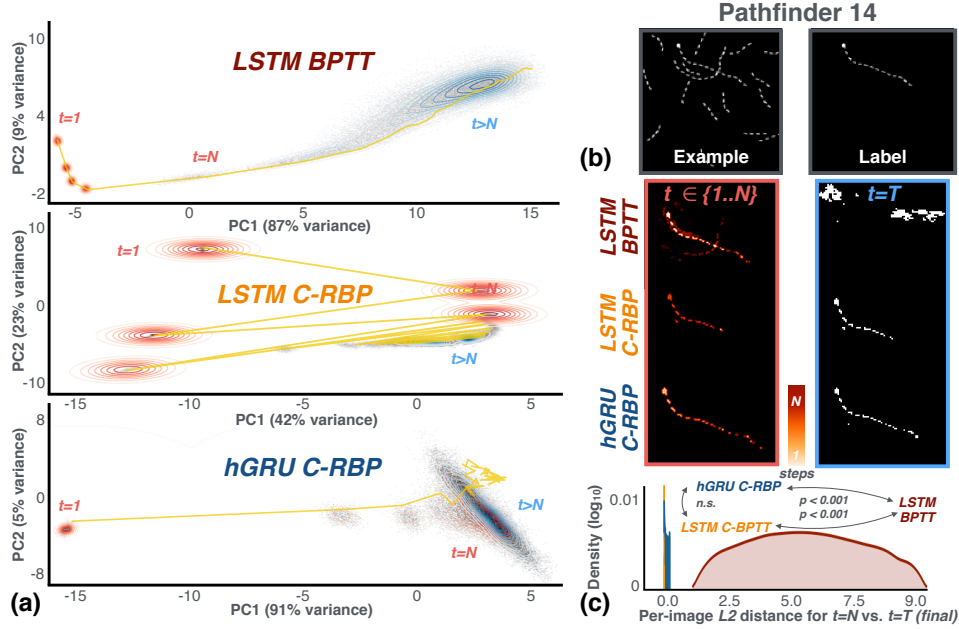


Figure S1: Convolutional LSTMs trained with (BPTT) exhibit unstable dynamics, like the BPTT-trained hGRUs examined in the main text. Once again, LCP corrects this pathology. (a) Visualization of convLSTM and hGRU state spaces following the state space method described in Section . Here, the BPTT-LSTM was trained for 6 steps, the C-RBP LSTM for 60 steps, and the C-RBP hGRU for 40 steps. Grey dots are the 2D-histogram of projected hidden states, red contours are hidden state densities up to the task-optimized N steps, and blue contours are hidden state densities beyond that point ($t > N$). Exemplar dynamics for a single image are plotted in yellow. While dynamics of the BPTT-trained model diverge when $t > N$, models trained with LCP did not. (b) Model dynamics are reflected in their performance on Pathfinder-14 at $t = N$ and $t = T$ steps of processing. (c) Two-sample KS-tests indicate that the distance in state space between $t = N$ and $t = T$ hidden states is significantly greater for the BPTT-trained convLSTM than for either of the models trained with C-RBP (n.s. = not significant).

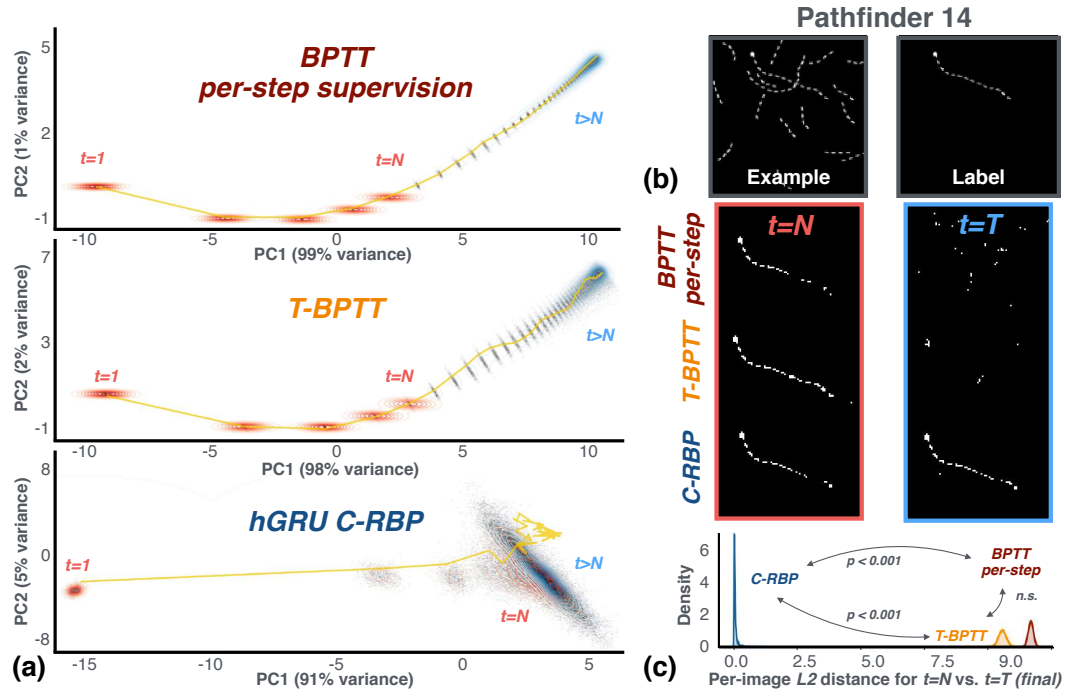


Figure S2: Additional state space analyses showed that alternatives to BPTT do not resolve the unstable dynamics we observed for recurrent CNNs. Here, **BPTT per-step supervision** refers to a model which was optimized with a loss evaluated on each of its 6 steps of processing. **CBPTT**-BPTT refers to a model trained with truncated backprop, for which gradients were accumulated over 3 steps of its 6 steps of processing. **(a,b,c)** The alternatives to train models with unstable dynamics, which causes task information to be forgotten after the optimized $t = N$ steps of processing. The distances between $t = N$ and $t = T$ hidden states are significantly greater for hGRUs trained with these algorithms than for an hGRU trained with **C-RBP** (*n.s.* = not significant).

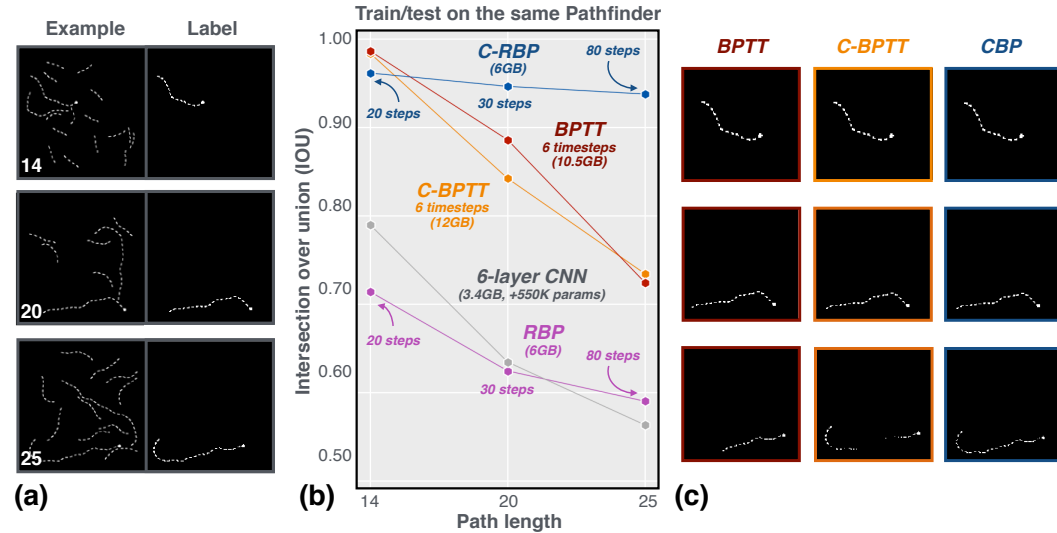


Figure S3: Exemplars from the (a) *Pathfinder* challenge, along with (b) model performance on each of these datasets, and (c) predicted contours from hGRUs trained with the different algorithms.

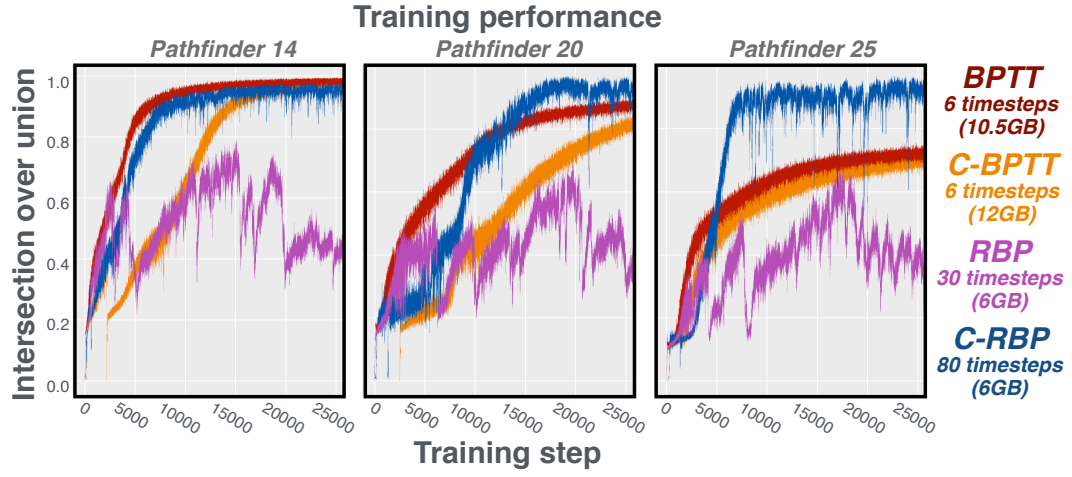


Figure S4: Performance of hGRUs during training on *Pathfinder* challenge datasets. The **RBP**-trained model struggles to fit any dataset, unlike the models trained with **BPTT**, **C-BPTT**, or **C-RBP**.

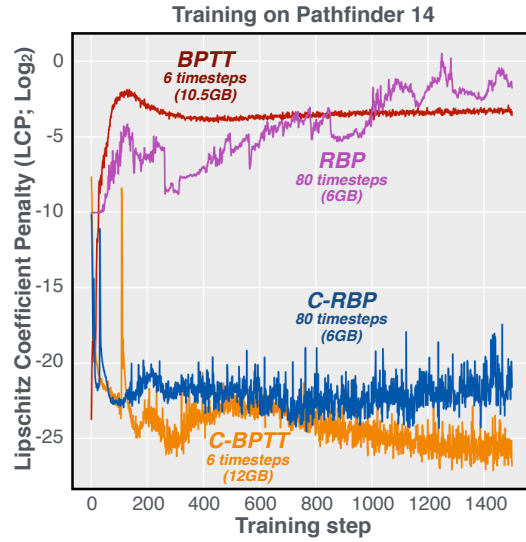


Figure S5: The value of our LCP (computed with Eq. 6 in the main text) over the course of training for models that minimize it (**C-RBP**, **C-BPTT**) and models that do not (**RBP**, **BPTT**). In other words, the magnitude of this correlates with the stability/instability of model dynamics.

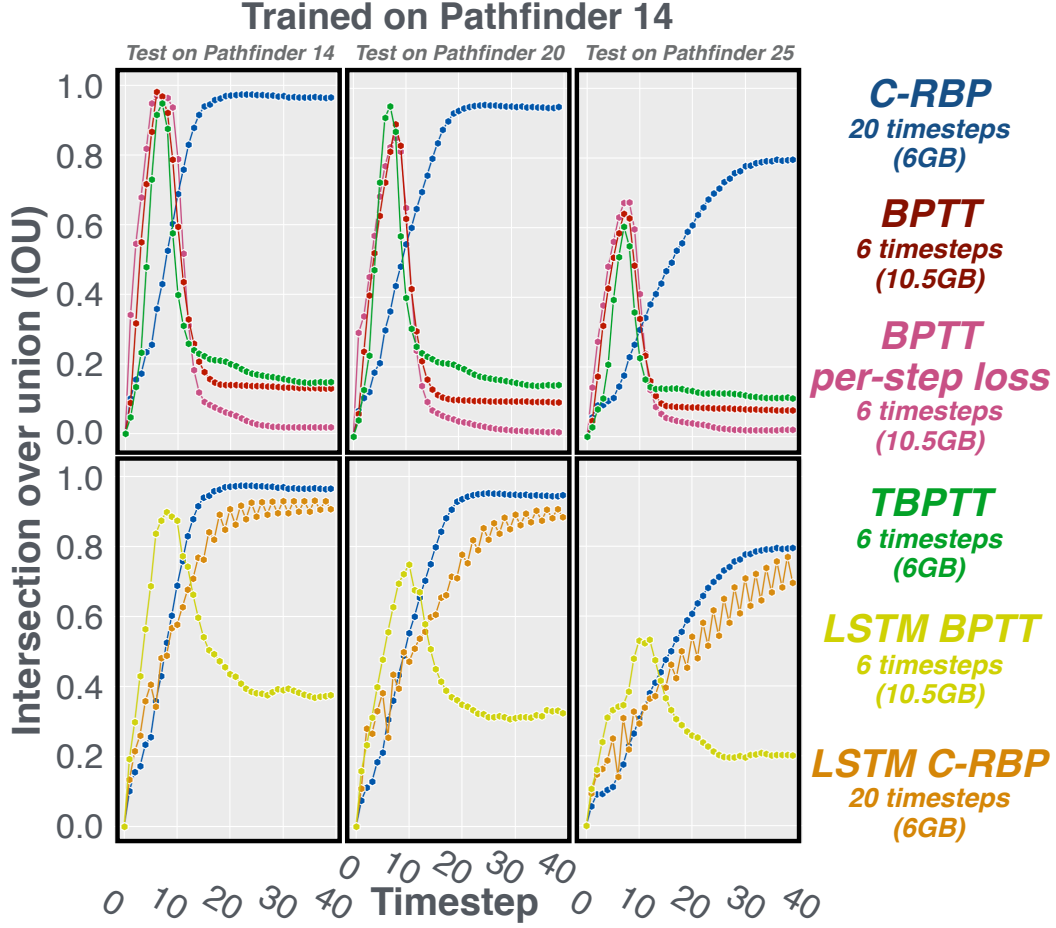


Figure S6: Generalization performance for hGRUs and convLSTMs trained with BPTT and alternatives to BPTT. Models were trained on Pathfinder 14 and tested on Pathfinder 14/20/25. For reference, performance of the hGRU trained with C-RBP is plotted in both rows. BPTT per-step loss means that a loss was computed on each of the 6 steps of hGRU training, and weights were optimized with BPTT. In contrast, a loss was only calculated on the final step for **BPTT**. TBPTT is truncated backprop through time, where gradients were computed over 3 steps of the 6 step dynamics. The LSTM trained with BPTT was trained for 6 steps, whereas the LSTM trained with C-RBP was trained for 60.

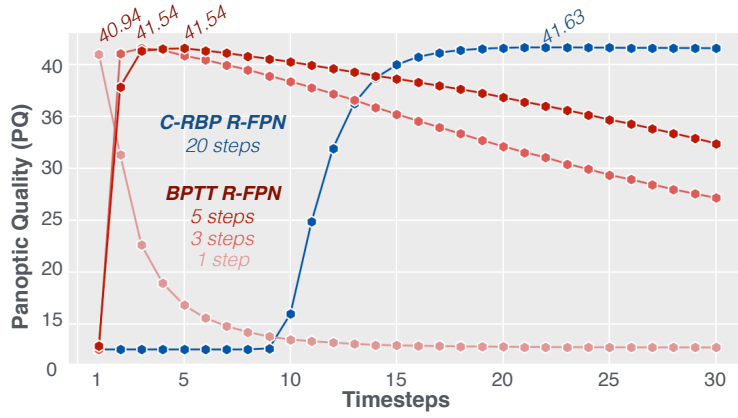


Figure S7: Recurrent model performance on MSCOCO Panoptic Segmentation. Performance was computed for each of 30 steps of processing for models trained with BPTT and C-RBP. The C-RBP models achieve better – and more stable – performance.

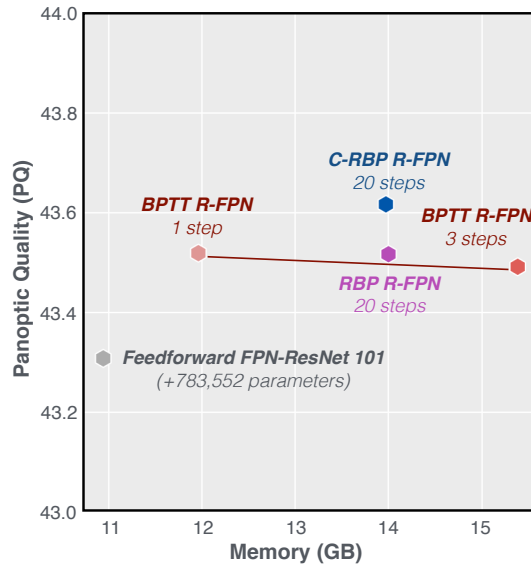


Figure S8: Our recurrent Panoptic Segmentation models also outperform the feedforward standard when both are given ResNet-101 backbones and the $3\times$ training schedule (see <https://bit.ly/dtcon> for details on this training routine). The C-RBP model, trained for 20 steps, outperforms any other tested version of the model.



Figure S9: Panoptic predictions from the feedforward ResNet-50 FPN Mask-RCNN (left) and our recurrent version of the model trained with C-RBP (right).

Feedforward FPN-ResNet 50

C-RBP Recurrent FPN-ResNet 50

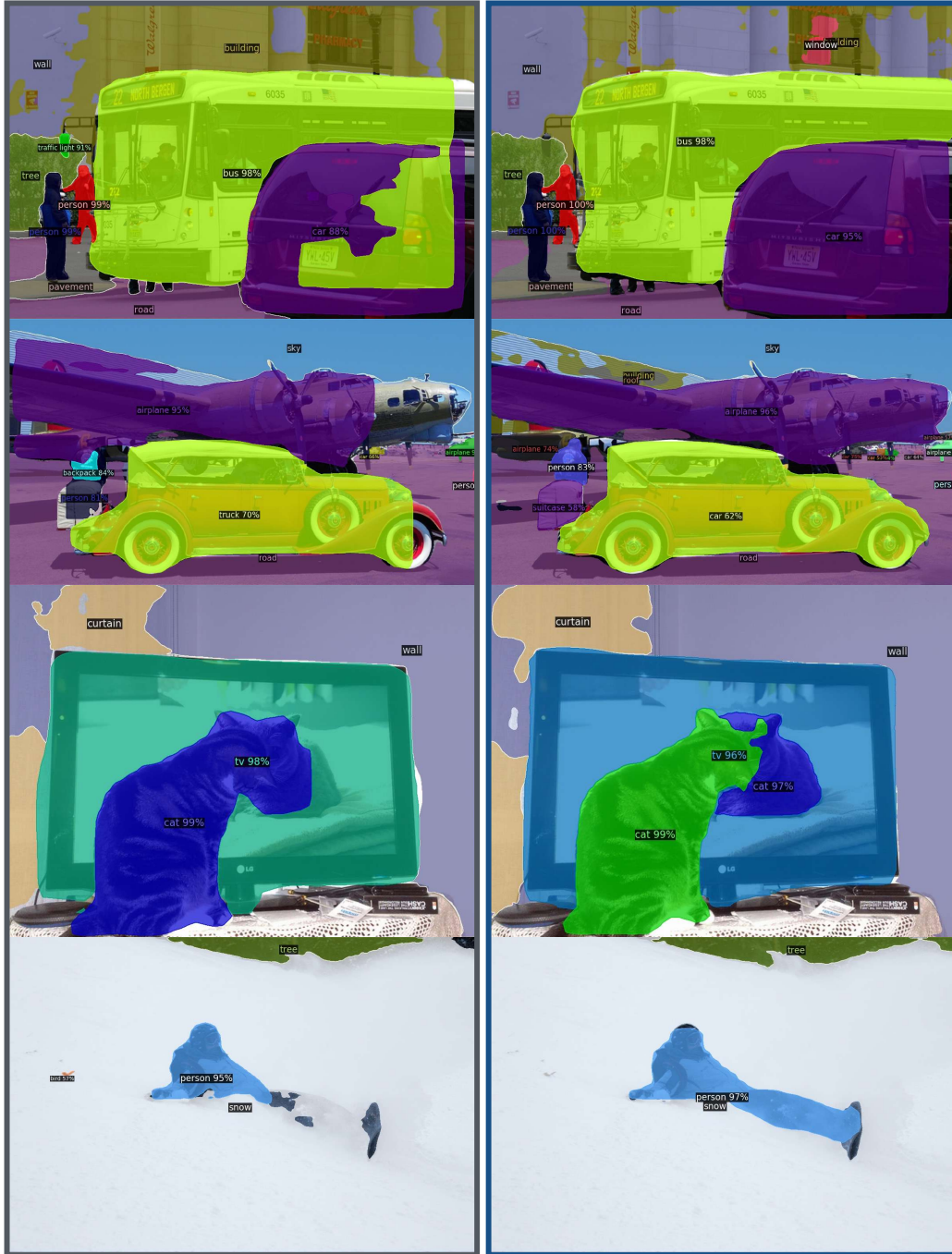


Figure S10: Panoptic predictions from the feedforward ResNet-50 FPN Mask-RCNN (left) and our recurrent version of the model trained with C-RBP (right).